Accuracy of Atmospheric Energy Budgets from Analyses

KEVIN E. TRENBERTH, DAVID P. STEPANIAK, AND JULIE M. CARON

National Center for Atmospheric Research, Boulder, Colorado*

(Manuscript received 17 December 2001, in final form 15 April 2002)

ABSTRACT

Issues relevant to achieving an accuracy of better than 10 W m^{-2} on 250-km scales for monthly means in the atmospheric energy balance are explored from the standpoint of the formulation and computational procedures using the National Centers for Environmental Prediction–National Center for Atmospheric Research (NCEP–NCAR, hereafter referred to as NCEP) and the European Centre for Medium-Range Weather Forecasts (ECMWF) reanalyses. The focus is on the vertically integrated energy components, their monthly tendencies, transports, and divergences, using the most accurate computations in model and pressure coordinates. Approximate equations have often been used previously; although relatively small compared with the moist static energy, kinetic energy transports should be taken into account, as divergences can exceed several tens of watts per square meter. Changes in energy storage terms over a month are not negligible, as they are typically over 25 W m^{-2} in storm track regions. Transports of energy are meaningful only if the mass budget is closed.

Typical magnitudes of the divergence of sensible heat and potential energy are very large (several hundred watts per square meter), but partly cancel when combined as dry static energy, reflecting the role of isentropic flow. The latent energy and sensible heat contributions are strongly positively correlated because of the dominance of low-level flow, and the latent energy divergence also cancels a large component of the dry static energy divergence, leaving a modest residual. This arises from the dominance of moist adiabatic processes in the Tropics and subtropics as the net divergent transports depend on temperature departures in the vertical from the saturated adiabatic lapse rate and their covariability with wind. Careful numerical treatments are required or else small errors in the large terms that should cancel can be amplified. Common assumptions that diagnostics can be computed on model terrain-following coordinates, which therefore vary from day to day as the surface pressure changes, lead to errors in energy budgets of the order of 5 W m^{-2} owing to the covariability of energy terms with surface pressure.

How well model coordinate results can be replicated in pressure coordinates has been explored along with the role of vertical resolution using a postprocessor developed at NCAR. The standard 17-level reanalysis pressure level archive does not adequately resolve the atmosphere, and we propose a new set of 30 pressure levels that has 25-mb vertical resolution below 700 mb and 50-mb vertical resolution in the rest of the troposphere. The diagnostics reveal major problems in the NCEP reanalyses in the stratosphere that are inherent in the model formulation, making them unsuitable for quantitative use for energetics in anything other than model coordinates. In addition, small flaws are found in the ECMWF postprocessing onto pressure levels. These stem from the way the vector fields are truncated, which is a necessary step to avoid aliasing before putting the values out on a 2.5° grid. Moreover, it is desirable to compute the gridpoint values exactly rather than interpolating them from the Gaussian grid, as currently done by ECMWF. The diagnostic results computed with 30 levels replicate the full model level vertically integrated energy divergences to within about 2 W m^{-2} over the ocean, while errors exceed 10 W m^{-2} in small spots over Greenland, Antarctica, and the Himalayan–Tibetan Plateau complex.

1. Introduction

A detailed knowledge of the heat budget of the climate system is desirable for improved modeling and understanding of climate variability. Achieving a monthly mean accuracy of better than 10 W m^{-2} in the energy balance on large scales (2° latitude by 5° longitude) is an oft-stated goal in programs such as Climate Variability and Predictability (CLIVAR; CLIVAR 1998), but is a major challenge to observations and diagnostic computations. This paper explores issues relevant to achieving this goal with the main focus on the formulation and computational procedures. Moreover, to focus on the important processes involved, a full description in three dimensions and as a function of time

* The National Center for Atmospheric Research is sponsored by the National Science Foundation.

Corresponding author address: Dr. Kevin E. Trenberth, NCAR, P. O. Box 3000, Boulder, CO 80307-3000.
E-mail: trenbert@ucar.edu

is desirable. For the atmosphere, in principle this can now be obtained from the reanalyses from the National Centers for Environmental Prediction–National Center for Atmospheric Research (NCEP–NCAR, hereafter referred to as NCEP) and the European Centre for Medium-Range Weather Forecasts (ECMWF). ECMWF reanalyses (ERA-15), are available for 1979–93, while the NCEP reanalyses begin in 1948 and are extended to the present using the Climate Data Assimilation System (CDAS). New reanalyses from ECMWF, known as ERA-40, extending over at least 40 years are in progress. In practice, attaining this complete description is not a simple task and the hazards are the subject of this paper.

We have previously made detailed computations of the vertically integrated heat, energy, and moisture budgets using the reanalyses (Trenberth and Guillemot 1998; Trenberth et al. 2001a; Trenberth and Caron 2001). In Trenberth et al. (2001a) we documented computations of monthly mean transports and tendencies in storage of all the relevant quantities, and compared the NCEP and ECMWF results. When combined with top-of-the-atmosphere (TOA) radiation data from the Earth Radiation Budget Experiment (ERBE) for February 1985–April 1989, implied surface fluxes and ocean heat transports can be computed and compared with other estimates (Trenberth and Caron 2001). The broadscale aspects and some details of both the divergence of atmospheric energy and the surface flux climatological means are reproducible between the NCEP and ECMWF results, especially in the zonal means, but differences are also readily apparent (Trenberth et al. 2001a). Overall, the surface fluxes and the implied ocean heat transports from NCEP reanalyses seem to be quite good and superior to those from ECMWF over the oceans (Trenberth et al. 2001a; Trenberth and Caron 2001). Therefore we explore reasons for the differences by examining individual components of the atmospheric energy.

To close the monthly energy budget to within 10 W m^{-2} on about 250-km scales it is vital to accurately formulate the energy equations and the components, to include all terms, including energy tendency terms, and pay special attention to numerics and consistency in diagnostic computations. As we show, several terms are very large but involve substantial cancellation, so that relatively small errors arising through inconsistent computations could result in large residual errors in the total budget.

Very often energy budgets are formulated with approximate equations that either leave out the kinetic energy equation (e.g., Yu et al. 1999) or more commonly formulate a dry static energy $s = c_pT + \Phi$ equation (e.g., Yanai et al. 1973, 1976) in which $s(x, y, p, t) = c_pT(x, y, p, t) + \Phi(p)$. Here c_pT is the sensible heat and Φ the geopotential. However, the subtlety of omitting the horizontal and time dependence in the geopotential part of the dry static energy can be missed. It is almost equivalent to dropping the kinetic energy component and has been perpetuated in many further studies, such as Tian et al. (2001, and references therein), while other studies ignore the heating from frictional dissipation (e.g., Johnson and Ciesielski 2000). Here we show that the transports of kinetic energy and their divergence, while relatively small compared with those of the moist static energy, are not negligible.

The NCEP reanalyses have been used to deduce the diabatic heating by Yanai and Tomita (1998), but they used the pressure level archive and only twice-daily values, so that the semidiurnal tide is aliased in their results and they are dependent on the accuracy of the postprocessing of data onto pressure levels—an issue explored later in this paper. Yu et al. (1999) used both NCEP and ECMWF reanalyses to compute zonal mean divergences of atmospheric energy transports, but they also use pressure level analyses on a 2.5° grid. One issue we pursue here is the accuracy of results from the pressure level archive.

Tendency terms are widely ignored on the grounds that averaging in time reduces them to become negligible. However, we find that this is not the case for monthly or seasonal timescales and, in addition, systematic variations with the annual cycle can be important. We document for the first time the magnitude of the tendency terms for individual months. These terms arise mostly from synoptic variability as manifested in large local changes between the observed state at the end versus the beginning of each month. However, they are small enough to ignore only with averages over many years.

In addition, in several other respects these computations are extremely demanding and are not straightforward. Substantial adjustments are required to the energy terms to obtain sensible results by requiring the mass budget to balance (Trenberth 1991, 1997). In fact, a prerequisite for determining the energy budget and energy transports is to have a balanced closed mass budget. Otherwise, there is an implied return flow, mandated by continuity, somewhere else that is transporting energy. This means that fluxes of energy in part of the atmosphere, such as the upper troposphere, should not be interpreted as transports because they do not take account of the return flow, such as in the lower troposphere in the Hadley circulation. Yet this is not an uncommon approach (e.g., Tian et al. 2001).

In addition, strong dynamical constraints on the flow mandate relationships among various energy components. If internal energy is increased through an increase in temperature, then the atmospheric column expands and thus alters the potential energy. Prior to condensation, atmospheric flow tends to be isentropic, and rising air cools at the dry adiabatic lapse rate, further ensuring a strong link between sensible heat and potential energy. The latter are combined in the concept of dry static energy. A parcel of air near sea level has high sensible heat and small potential energy, but when lifted to the upper troposphere, sensible heat is lost through adiabatic cooling while the potential energy increases.

Also, low-level mass divergence has to be compensated by upper-level mass convergence, or vice versa, so that the divergence of energy fluxes has enormous compensation in the vertical by design. Similar concepts apply when condensation takes place, except that a rising air parcel cools at the saturated adiabatic lapse rate, and, as we show in section 3, it is the departures from the saturated adiabatic lapse rate in the vertical and their covariability with velocity that determine net meridional energy transports. Other diabatic processes generally act on slower timescales and are of less consequence.

The full-resolution 4 times daily data on model coordinates have been used to obtain the best accuracy possible. The processing of 1 month of 4 times daily ECMWF ERA-15 analyses on 31 model levels at T106 resolution of data required 8 h of time on an SGI machine (SGI Power Challenge XL 10000; 8 processors and 1 GB of memory), largely because of the huge volumes of input and output required. With prospects of the ERA-40 reanalyses being at T159 resolution and 60 levels, there is interest in how well results can be replicated with the pressure level archive. Hence, we have similarly processed the NCEP and ECMWF pressure level data, which are more readily available and which constitute a much smaller processing task as they are on a 2.5° grid at 17 levels. These then provide products that can be compared with the complete results and evaluated to determine the effects of vertical interpolation to the pressure levels and degraded horizontal and vertical resolution. Replication of the full results, reported on here, is a necessary condition before we can have confidence in a breakdown of the vertically integrated transports into contributions by layers.

To further explore the sources of errors, we have developed a postprocessor of the model level data to recreate the pressure level archive, and thus we have also developed the capability to create a pressure archive at much higher vertical resolution, for instance with pressure layers of 25 mb throughout the troposphere. In this way we can address issues related to how well the surface and the topography are resolved and explore other sources of discrepancies.

The results have implications, not only for diagnostic computations, such as in this paper, but also for modeling, postprocessing model data, and analyses. Comments are made on the utility of sigma (as in the NCEP model), hybrid (as in the ECMWF model), and pressure coordinates. Sigma coordinates are terrain-following coordinates where the surface pressure is the first level, and all other levels are normalized by the surface pressure. Hybrid coordinates are similar at the bottom of the atmosphere but transition to pressure levels in the stratosphere, somewhere near 100 mb. Consequently there are issues relating to the interpolation from one vertical coordinate to another, and how to define time averages when the surface pressure and thus the coordinate system is varying in time. Dividing the atmosphere up into model layers, as is commonly done by modelers in computing diagnostics, does not take the varying coordinate system into account. During the course of this study, we have also discovered several other problems in how data are postprocessed and archived on pressure levels.

In this paper we focus on the vertically integrated energy budget as a key diagnostic. Section 2 briefly discusses the datasets used. The physical background and mathematical expressions for the transports and their components are given in section 3. In section 4 we break the total energy transport down into the components of sensible heat and potential energy that make up the dry static energy, latent energy, and kinetic energy. We then explore the importance of the tendency terms in section 5 and go on to examine how well they can be replicated with the pressure level archives in section 6. The conclusions are given in section 7.

2. Data

The reanalyses from NCEP–NCAR (Kalnay et al. 1996) and ECMWF (Gibson et al. 1997) have been used to compute the vertically integrated atmospheric mass, heat, energy, and moisture budgets for 1979–93 and with an extension for NCEP data through 2000. The global analyses are produced on model (sigma or hybrid) surfaces that consist, in simplest form, of a sigma (σ) terrain-following coordinate in which the lowest level corresponds to $p = p_s$, where p is pressure, p_s is the surface pressure, and $\sigma = p/p_s$. Hybrid η coordinates consist of σ near the surface but with a gradual transition to pressure with height.

The NCEP system is based on a numerical weather prediction model with T62 spectral resolution and 28 sigma levels in the vertical with 5 of those levels in the atmospheric boundary layer (Table 1). The ''half levels'' are defined in the model (Kalnay et al. 1996) and are not halfway between the full levels either linearly in p or ln$p$; the layers defined by the half levels are also given in Table 1. Fields are not initialized. Trenberth and Guillemot (1998) provide an evaluation of the NCEP reanalyses from the standpoint of the hydrological cycle.

The ECMWF reanalyses are at T106 resolution and 31 levels in the vertical with a hybrid coordinate that transitions to a pressure coordinate above about 100 mb (Table 1). The u, v, T, and RH fields are given on the full levels while the geopotential is on the half levels. However, there are continuity problems with the ECMWF reanalyses arising from the positive reinforcement of biases in satellite radiances with those of the assimilating model first guess (Stendel et al. 2000; Trenberth et al. 2001b). Two spurious discontinuities are present in tropical temperatures and humidity, with jumps to warmer values throughout the Tropics below 500 mb in late 1986 and early 1989, and further spurious interannual variability is also present. These aspects are

TABLE 1. The vertical coordinates for the ECMWF and NCEP reanalysis models for an assumed surface pressure of 1000 mb. Shown are the model levels at which the main variables (u, v, T, RH) are defined in the analyses, although T is derived from z, which is on the half levels (not shown) for (left) ECMWF and (right) NCEP. The thickness of the pressure layers dp resulting from the half-level values are also given along with the pressure archive levels. In the pressure archives, ECMWF includes 775 but not 20 mb, while NCEP includes 20 but not 775 mb.

ECMWF			Pressure	NCEP		
Level	dp	p	p	p	dp	Level
				0		0
0		0		2.7	6.6	1
1	20.0	10.0	10	10.1	7.3	2
			(20)	18.3	9.2	3
2	20.0	28.9	30	28.8	11.6	4
3	20.0	49.3	50	41.8	14.5	5
4	20.0	69.5	70	58.0	18.0	6
5	20.2	89.7		78.2	22.2	7
6	21.0	110.3	100	102.8	27.1	8
7	22.4	132.0		132.6	32.7	9
8	24.2	155.3	150	168.2	38.6	10
9	26.2	180.5				
10	28.3	207.7	200	210.1	45.1	11
11	30.4	237.0	250	258.2	51.3	12
12	32.4	268.4				
13	34.4	301.8	300	312.5	57.2	13
14	36.2	337.1				
15	37.9	374.2		372.0	61.9	14
16	39.4	412.9	400	435.7	65.3	15
17	40.9	453.0				
18	42.2	494.5	500	501.7	66.7	16
19	43.3	537.3				
20	44.3	581.1	600	568.1	66.0	17
21	45.0	625.8		632.9	63.5	18
22	45.5	671.1	700	694.3	59.2	19
23	45.6	716.6		750.8	53.7	20
24	45.2	762.1	(775)	801.4	47.6	21
25	44.2	806.8		845.8	41.1	22
26	42.2	850.1	850	883.8	34.9	23
27	39.1	890.7		915.9	29.2	24
28	34.5	927.6	925	942.5	24.1	25
29	28.1	958.9		964.4	19.6	26
30	19.3	982.6		982.1	15.8	27
31	7.7	996.1		995.0	10.0	28
Ps		1000.0	1000	1000.0		Ps

not relevant to the current analysis that focuses on January 1989.

Note that the model levels contain much greater vertical resolution than the standard pressure levels in the boundary layer in both models (Table 1); the ECMWF vertical resolution is higher than for NCEP in the mid- to upper troposphere, and the NCEP model has extra levels in the stratosphere. In this table the model levels are given for a surface pressure of 1000 mb, and only the ECMWF model levels 1–5 are fixed. The need for improved resolution in the stratosphere has been recognized in both NCEP and ECMWF operational models, and the ERA-40 model will have 60 levels.

In the pressure coordinate archive, the 17 levels available from the reanalyses are p = 1000, 925, 850, 700, 600, 500, 400, 300, 250, 200, 150, 100, 70, 50, 30, 20, and 10 mb from NCEP; while ECMWF includes a 775-mb level but does not have a 20-mb level (see Table 1 for how the pressure levels lie relative to the model levels). We define the half levels as the average value of the standard levels. We have varied this by also taking the geometric average (or equivalently linear in ln$p$), which is closer to that of the model layers, but the differences on our computations are very small. For instance, for the 850- and 700-mb levels, the arithmetic mean midpoint is 775 mb, while the geometric mean is 771.4 mb. The half pressure levels are not shown in Fig. 1, but their difference, indicating the layer, as dp is given.

The computations were first performed in model coordinates at full resolution using 4 times daily analyses in order to produce vertically integrated quantities. Subsequently, the computations are redone using the pressure level archive that can then be used to explore more fully the vertical structure and relationships as a function of pressure level.

3. Physical framework

a. Vertical integrals

The mass-weighted vertical integral of any quantity M integrated in the vertical over the mass of the atmosphere from the bottom ($p = p_s$, $z = 0$) to the top ($p = 0$, $z = \infty$) is given by

$$\tilde{M} = \int_0^\infty \rho M \, dz = \frac{1}{g}\int_0^{p_s} M \, dp = \frac{1}{g}\int_{\eta_s}^{\eta_t} \frac{\partial p}{\partial \eta} M \, d\eta, \quad (1)$$

where η_t corresponds to $p = 0$ and η_s corresponds to $p = p_s$. The $\partial p/\partial \eta$ plays the role of a density factor in these coordinates. In the event that σ is the vertical coordinate, this mass-weighting factor becomes p_s.

b. Mass budgets

For water vapor the mass budget is

$$\frac{\partial w}{\partial t} + \nabla \cdot \frac{1}{g}\int_0^{p_s} q\mathbf{v} \, dp = E - P, \quad (2)$$

where the precipitable water $w = 1/g \int_0^{p_s} q \, dp$. Here E is the rate of evaporation and P is precipitation rate per unit mass, and we have ignored other forms of liquid and frozen water in the atmosphere.

For total mass of the atmosphere, the appropriate balance is

$$\frac{\partial p_s}{\partial t} + \nabla \cdot \int_0^{p_s} \mathbf{v} \, dp = g(E - P). \quad (3)$$

The right-hand side is typically ignored but this could contribute to heat budget errors of ~10 W m^{-2} (Trenberth 1997). Substantial adjustments are required to bal-

ance the mass budget, and we use the method given in Trenberth (1991).

c. Energy budget

Energy in the atmosphere occurs as kinetic energy $K_E = \tilde{k}$, internal energy $I_E = \widetilde{c_pT}$, potential energy $P_E = \tilde{\Phi}$, and latent energy $L_E = \widetilde{Lq}$. Here c_v is the specific heat at constant volume and L is the latent heat of vaporization. When integrated over the entire mass of the atmosphere, the total energy $T_E = I_E + K_E + P_E + L_E$ is conserved in the absence of heating and friction. The full energy equations are given in Trenberth (1997).

P_E is given by

$$P_E = \int_0^\infty gz\rho \, dz = \frac{1}{g}\int_0^{p_s} \Phi \, dp$$
$$= \frac{1}{g}\int_0^{p_s} (RT + \Phi_s) \, dp = \frac{R}{c_v} I_E + z_s p_s, \quad (4)$$

after integrating by parts and using the equation of state and hydrostatic equation, and where R is the gas constant, Φ_s, the surface geopotential, is not a function of pressure, and z_s, is the surface geopotential height. Hence,

$$T_E = \frac{1}{g}\int_0^{p_s} (c_pT + k + Lq + \Phi_s) \, dp, \quad (5)$$

where c_p is the specific heat at constant pressure. The R and c_p vary with the amount of moisture in the atmosphere, but it is a good approximation to treat them as constant.

Combining the vertically integrated dry and moist energy equations through the atmospheric column (Trenberth 1997), gives

$$\frac{\partial}{\partial t} T_E + \nabla \cdot \mathbf{F}_A = \tilde{Q}_1 - \tilde{Q}_2 - \tilde{Q}_f, \quad (6)$$

where

$$\mathbf{F}_A = \frac{1}{g}\int_0^{p_s} (h + k)\mathbf{v} \, dp \quad (7)$$

is the atmospheric energy transport, $h = s + Lq$ is the moist static energy, and $s = c_pT + \Phi$ is the dry static energy. Also $\tilde{Q}_1$ is the diabatic heating, $\tilde{Q}_f$ is the frictional heating arising from dissipation of kinetic energy, and $\tilde{Q}_2 = L(P - E)$ is the column latent heating. Global mean $\tilde{Q}_f$ is estimated to be 1.9 W m^{-2} by Oort and Peixoto (1983), and, hence, is very small.

The first term in (6) is the change in energy storage in the atmosphere, the second term is the total atmospheric energy transport divergence. Note that the second term is not simply the divergence of internal, potential, kinetic, and latent energy, as it includes the pressure-work term in the thermodynamic equation. In section 4 we present results of $\nabla \cdot \mathbf{F}_A$ broken down into the basic terms. Hence, we include results for divergences of transports of the following: sensible heat $\widetilde{c_pT}$; potential energy $\tilde{\Phi}$; the dry static energy $\tilde{s}$, which is their sum; the latent energy $\widetilde{L_q}$; the sum of the latter two as the moist static energy $\tilde{h}$; the kinetic energy $\tilde{k}$; and the total energy ($\widetilde{h+k}$). It is the divergence of the latter that is linked to the energy sources and sinks in the atmosphere.

Because mass is conserved, ignoring the surface pressure variations

$$\nabla \cdot \frac{1}{g}\int_0^{p_s} \mathbf{v} \, dp \approx 0, \quad (8)$$

and this can be compared with the expression for divergence of atmospheric energy transport

$$\nabla \cdot \mathbf{F}_A = \nabla \cdot \frac{1}{g}\int_0^{p_s} (h + k)\mathbf{v} \, dp, \quad (9)$$

which is identical on the rhs except for the $(h + k)$ factor. Moreover, k is small compared with h, and so it is the departures of h in the vertical from a constant value and their correlation with velocity that contribute to the energy transports. In regions where transient eddy effects are minor, such as the Tropics, this interpretation can also be applied to the time-averaged flow. Because $h = c_pT + gz + Lq$,

$$\frac{\partial h}{\partial p} = c_p\left[\frac{\partial T}{\partial p}\left(1 + \frac{L}{c_p}\frac{\partial q}{\partial T}\right) - \frac{g}{c_p}\frac{RT}{p}\right]. \quad (10)$$

When the expression on the rhs is set to zero, so that h is constant with height, but with q replaced by q_s (which depends on T), we obtain the saturated adiabatic lapse rate. Hence the profile for h_s is constant for the saturated adiabatic lapse rate, and so the profile of departures of h from this value factors into divergence of the atmospheric energy transport. Instead of the moist static energy, other expressions use the ''saturation entropy'' (see Emanuel 1995), and both are related to the equivalent potential temperature.

d. p versus model coordinates

The lowest model level typically does not coincide with that of the real surface; it varies with resolution and differs from one model to another. This means that model results cannot be compared unless they are placed on a common vertical coordinate, and the only one that makes sense is pressure. There are additional issues in using model coordinates.

It is common practice in examining model results or analyses in model coordinates to compute time averages on the model surfaces. However, the model surfaces are not fixed because the surface pressure varies. As a time average is performed, the surface pressure and thus the model coordinate itself also becomes time averaged. We

have performed most computations of $\nabla \cdot \mathbf{F}_A$ and its components in (7) using this flawed approach of computing the flux, time averaging over a month, then vertically integrating, and finally computing the divergence. These results are given in section 4a. We label these ''TI'' to denote ''time average'' then ''integrate.'' We also tried the reverse operation, which is more accurate but also much more burdensome, whereby the vertical integral is done every 6 h and then the monthly mean statistics are computed, labeled ''IT''; see section 4b. The differences between these approaches are therefore associated with covariability of the energetics with surface pressure (Trenberth 1995).

4. Comparisons among different computations in model coordinates

We focus on $\nabla \cdot \mathbf{F}_A$ as the primary quantity of interest and we use a single month, that of January 1989, to carry out most of the experimentation and to illustrate the results.

a. Energy components

Figure 1 shows $\nabla \cdot \mathbf{F}_A$ from the full TI model integrations for ECMWF and NCEP for January 1989. There are substantial differences, as shown in Fig. 1 (bottom) which exceed 60 W m^{-2} in many areas and are fairly typical of other months (see Trenberth et al. 2001a). Mass corrections, based upon the method of Trenberth (1991), required adjustments to the barotropic divergent wind component, of slightly more than 0.2 m s^{-1} for NCEP and about 0.1 m s^{-1} for ECMWF. For NCEP this corresponds to a divergence of 10^{-7} s^{-1}. The effects on the energy budget can exceed 100 W m^{-2} (Trenberth 1997).

The divergence of various TI transport components from ECMWF are given in Fig. 2 for sensible heat (SH) and potential energy (PE), and their sum, the dry static energy (DSE). Figure 3 shows results for the kinetic energy (KE), and the latent energy (LE) component is given in Fig. 4. Contributions from the two components of the DSE have very large contributions (contour interval 200 W m^{-2}) that tend to cancel, so that their sum is about one-third of the individual terms (contour interval 50 W m^{-2}). The cancellation arises from the dry adiabatic lapse rate combined with the opposite values of divergence in the upper and lower troposphere [because of (8)]. Thus temperatures are large in the lower troposphere where geopotential height is small, while temperatures are low in the upper troposphere where geopotential height is large. They are related through a relatively constant potential temperature. This cancellation requires very strict adherence to the hydrostatic relationship between temperature and geopotential in finite difference schemes or else discrepancies can readily arise in energy diagnostics. This was a source of problems in earlier budget computations where geopotential and temperature were processed separately, especially in computing zonal means from radiosonde observations (e.g., Oort 1978). It can also be a source of problems in pressure level archives: only temperature or geopotential height should be interpolated and the other derived in the new coordinate system.

However, there is a strong positive correlation between the moist component of the energy divergence and that of the sensible heat (cf. Fig. 4b with 2a). This occurs because most moisture is at low levels, and the low-level divergence field operates on both boundary layer moisture and sensible heat. Hence there is also a strong cancellation between the moist component and the dry static energy divergences (Fig. 4b versus 2c). So this cancellation is linked to vertical gradients of the moist static energy and relates to the departures from the saturated adiabatic lapse rate, as given by (10); see the discussion in section 3.

Contributions of kinetic energy to the total energy divergence (Fig. 3) are much smaller than the other terms, but not negligible. The term has values of several tens of watts per square meter focused along the winter jet stream with structures indicating entrance and exit regions of the northern jets. Differences with NCEP are typically $\sim$3 W m^{-2}.

The latent energy divergence is related to $E - P$ except for small tendency terms, see Eq. (2) (recall 29 W m^{-2} is about 1 mm day^{-1}). A detailed evaluation of $E - P$ from the moisture budget versus E and P from the model and independent estimates of P was given by Trenberth and Guillemot (1998) for the NCEP reanalyses. Differences in $E - P$ between the two reanalyses are large (Stendel and Arpe 1997), and this is also true for our example for January 1989 (Fig. 4c). Differences are very dependent on the fidelity of the low-level divergence field, which differs greatly between the two reanalyses on a month by month basis, although the mean annual cycle has some resemblance (Trenberth et al. 2000). To help evaluate the fields in Fig. 4, Fig. 5 presents the estimate of precipitation P from Xie and Arkin (1996, 1997). Evaporation does not vary as much temporally or spatially as P, although there are clear differences between land and ocean. Values over the oceans range from 2 to about 6 mm day^{-1} except off the east coasts of Asia and North America (Trenberth and Guillemot 1998). Therefore the structure of $E - P$ tends to be dominated by that of P.

For January 1989, differences in the latent energy divergence between NCEP and ECMWF (Fig. 4) are typically about 40 W m^{-2} in the Tropics although they range from -100 to 175 W m^{-2}. Zonal mean differences (not shown) peak at about 15 W m^{-2} near 13°N with ECMWF values being larger than NCEP. We have integrated these differences from the north and find that the smaller ECMWF Northern Hemisphere northward atmospheric energy transports of Trenberth and Caron (2001) appear to be largely accounted for by the latent

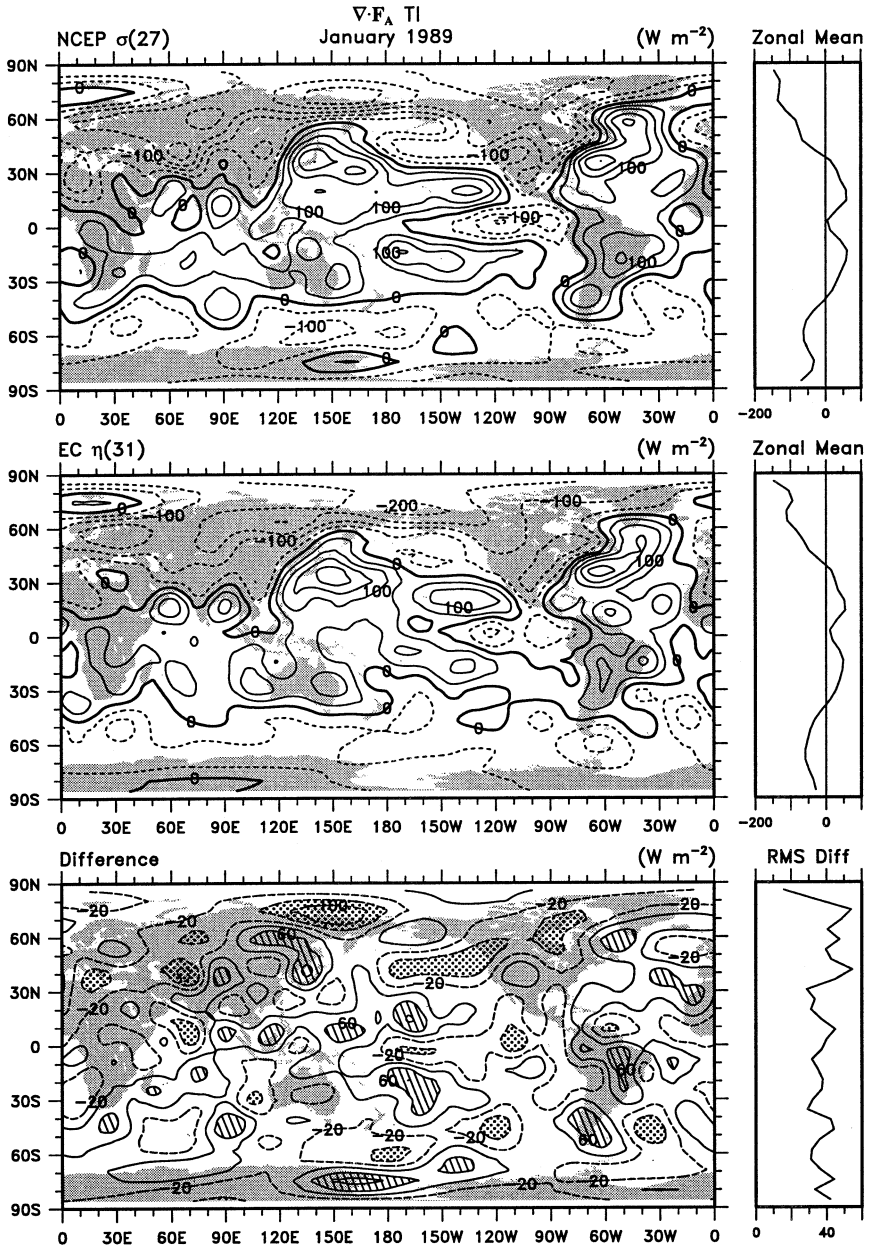

FIG. 1. Vertically integrated $\nabla \cdot \mathbf{F}_A$ for (top) NCEP, (middle) ECMWF, and (bottom) their difference, from the full model coordinate TI computations for Jan 1989. The fields are truncated at T21 resolution to show the larger-scale features. The contour interval is 50 W m^{-2} in the (top) and (middle) and 40 W m^{-2} in the (bottom). Panels showing zonal means are given at right except zonal mean rms differences are given at bottom right. Negative values are dashed. In (bottom) values >60 W m^{-2} are hatched and <-60 W m^{-2} are stippled.

energy component (differences as much as 0.5 PW), at least in this month.

The rms differences around a latitude circle are very large over tropical land in the monsoonal rain areas in the Southern Hemisphere (80 W m^{-2} or about 2.75 mm day^{-1} at 10°S), and about half these values over the ocean, so the overall zonal mean rms differences peak at ~60 W m^{-2} (Fig. 4). Neither reanalysis captures the double South Pacific convergence zone (SPCZ) structure (Fig. 5) for this month. The ECMWF values imply much larger P in the SPCZ than for NCEP and, while the latter appear to be underestimated, the former may be too large. The NCEP $E - P$ features a minimum near 10°N, 140°W, which corresponds much better to the observed P than in the ECMWF field. Otherwise, there is qualitative agreement of both latent energy divergences with the P field in spite of their large differences.

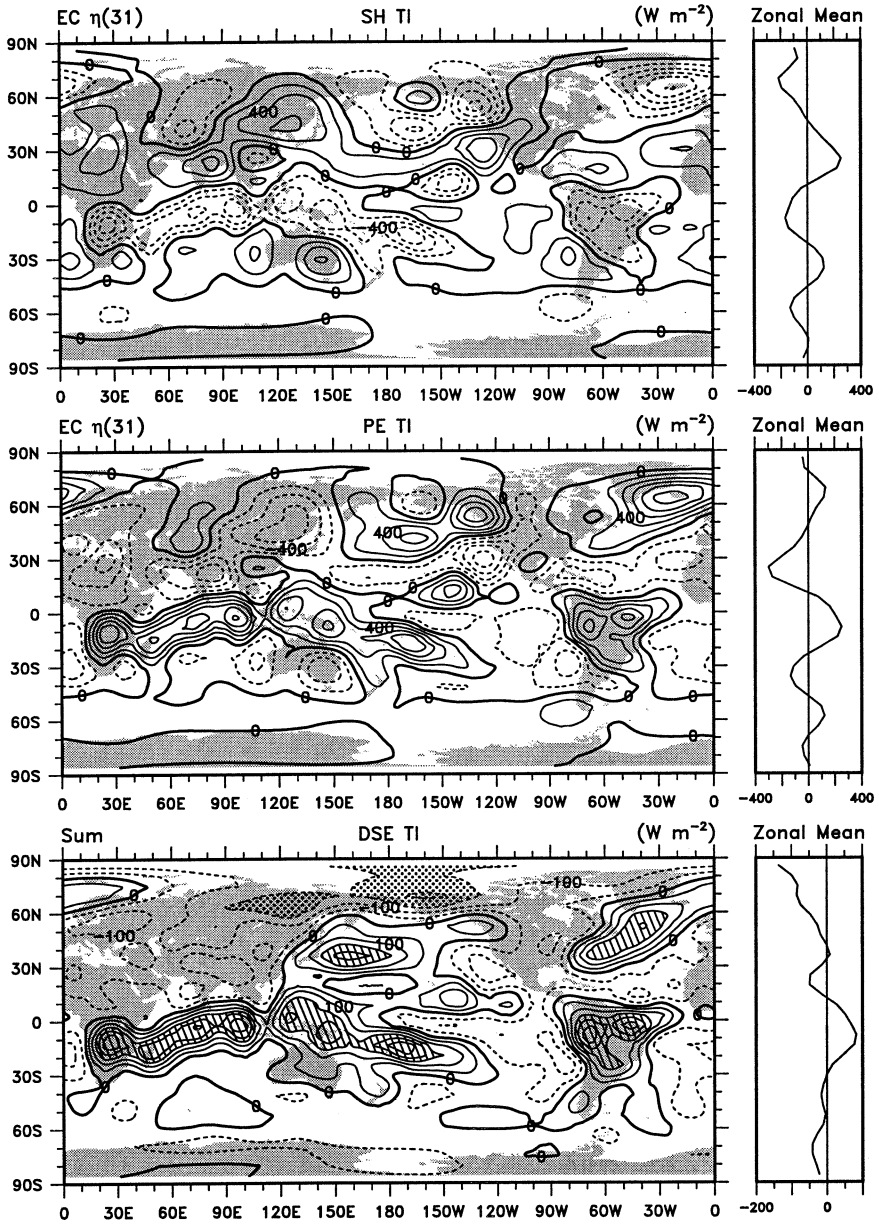

FIG. 2. Components of vertically integrated TI $\nabla \cdot \mathbf{F}_A$ from ECMWF from (top) sensible heat, (middle) potential energy, and (bottom) their sum, the dry static energy for Jan 1989. The contour interval is 200 W m^{-2} in the (top) and (middle). The contour interval is 50 W m^{-2} in the (bottom) and values $>$150 W m^{-2} are hatched and $<-$150 W m^{-2} are stippled. The zonal means are given at right.

To summarize, the total vertically integrated atmospheric energy is dominated by the moist static energy, while the kinetic energy contribution is small, but not negligible. The moist static energy divergence, in turn, consists of large components from the latent and dry static energies that tend to cancel leaving a smaller residual. Further there is very large cancellation between the sensible heat and potential energy contributions to the dry static energy, so that it is important that these be computed together in a consistent way (as is done automatically in an isentropic framework), or large errors can result. It is misleading to focus on only one of these components, as has been done in some studies (e.g., Tian et al. 2001).

b. Within-month variations in the model coordinate

Instead of using the monthly mean surface pressure as the coordinate, we also vertically integrated at each time to give the more accurate IT results (Fig. 6), and

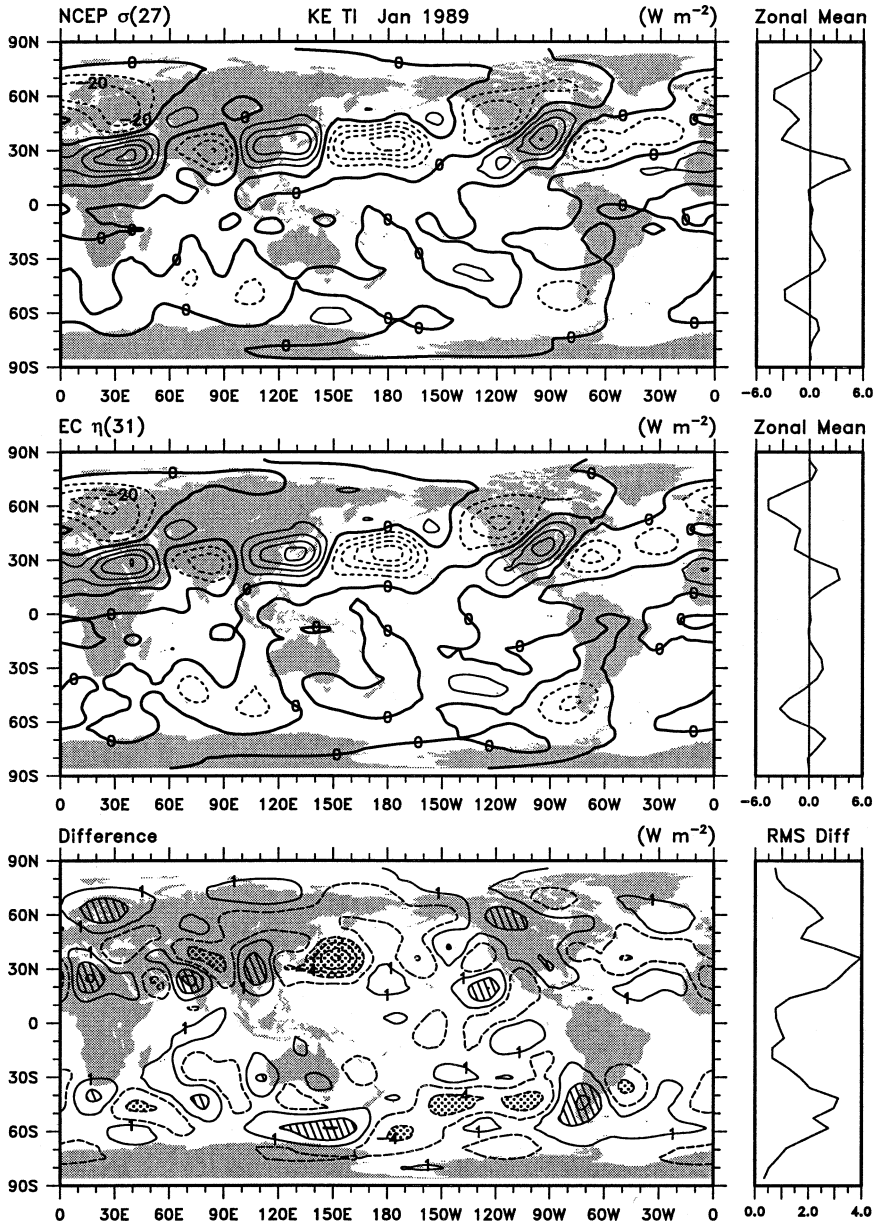

FIG. 3. Components of vertically integrated TI $\nabla \cdot \mathbf{F}_A$ from kinetic energy for (top) NCEP, (middle) ECMWF, and (bottom) their difference. The contour interval is 10 W m^{-2} in the (top) and (middle), and ± 1, ± 4, ± 7, etc., in the (bottom) with values >4 W m^{-2} hatched and <-4 W m^{-2} stippled. Panels showing zonal means are given at right except the bottom right panel shows zonal mean rms differences.

differences range from -8 to $+8$ W m^{-2} mainly over the storm tracks of the Northern Hemisphere oceans for January 1989. Although Trenberth et al. (2001a) used the results equivalent to those in Fig. 1a as the basis for their comparison and evaluation, the difference (Fig. 6b) is common to both reanalyses. However, the result in Fig. 6a is the most accurate and complete one, and, hence, forms the basis for the evaluation of the results in pressure coordinates.

5. Monthly storage tendency terms

We define a month as the mean of the 4 times daily fields beginning 0000 UTC on the first to 1800 UTC on the last day of the month. Accordingly, the month actually represents the period between 2100 UTC on the last day of the month and 2100 UTC on the last day of the previous month. We obtain the 2100 UTC value as the mean of the values at 1800 and 0000 UTC. The tendency is then the difference divided by the time.

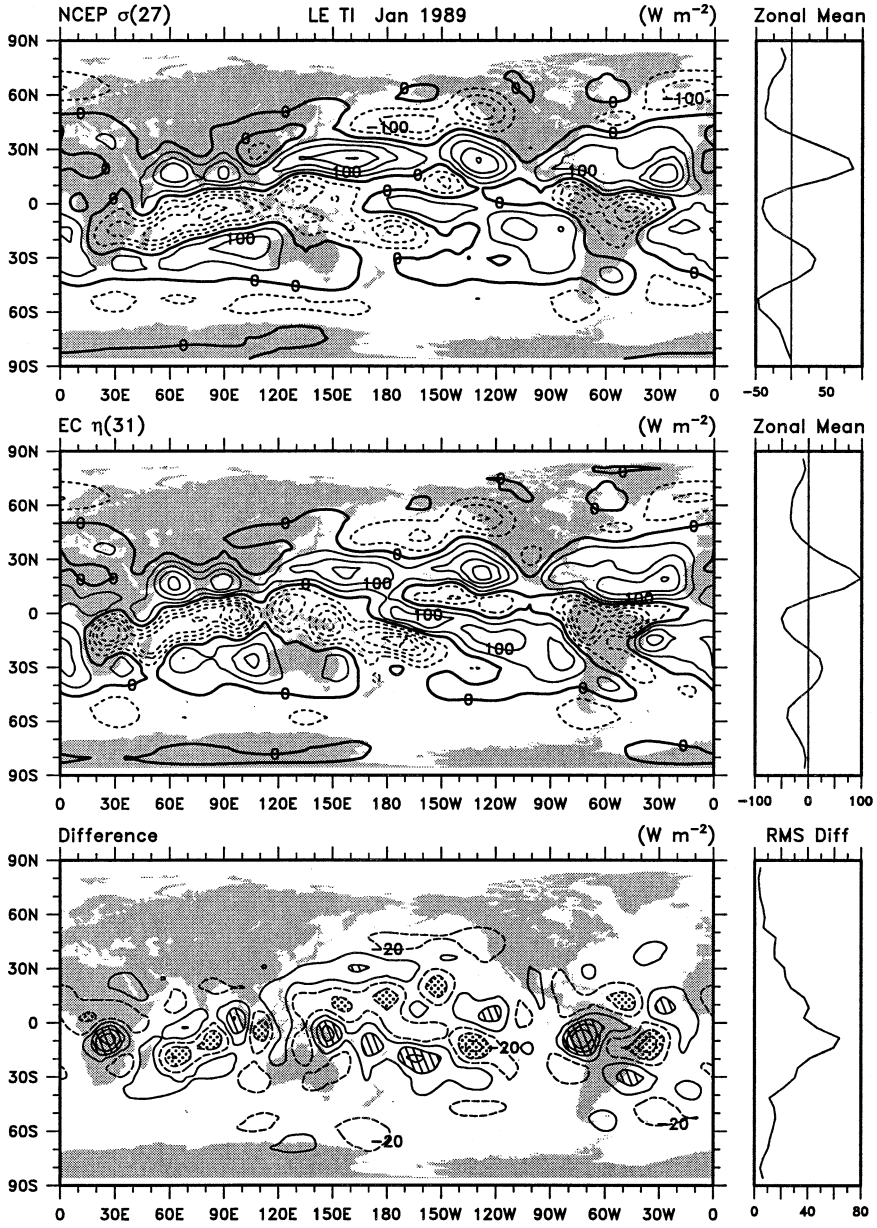

FIG. 4. Components of vertically integrated TI $\nabla \cdot \mathbf{F}_A$ from latent energy from (top) NCEP, (middle) ECMWF, and (bottom) their difference. The contour interval is 50 W m^{-2} in the (top) and (middle), and 40 W m^{-2} in the (bottom) with values >60 W m^{-2} hatched and <-60 W m^{-2} stippled. Panels showing zonal means are given at right except the values are zonal mean rms differences in the bottom right panel.

It has often been assumed for averages over a month or longer that changes in the storage of mass, moisture, or energy are sufficiently small that they can be neglected. Of course, the magnitude of these tendency terms diminish with the length of the time average. In Fig. 7 we show the annual mean of the standard deviation of monthly tendency terms for surface pressure, expressed as mb day^{-1}, and the effect on the surface geopotential energy term. This reflects the daily standard deviation for individual months. The zonal mean annual cycle is shown in Fig. 8. Values are nearly double those of Fig. 7 in January in the extratropics of the Northern Hemisphere but somewhat less in July. In the North Pacific, for instance, values range from 0.5 mb day^{-1} in July to 1.0 mb day^{-1} in January. In the Southern Hemisphere, the values are greatest in the winter and spring, but are more nearly uniform with time of year.

This variability is also manifested as variability of the sigma coordinate system and is directly felt in the Φ_s term in (5) when expressed as a tendency in (6), see Fig.

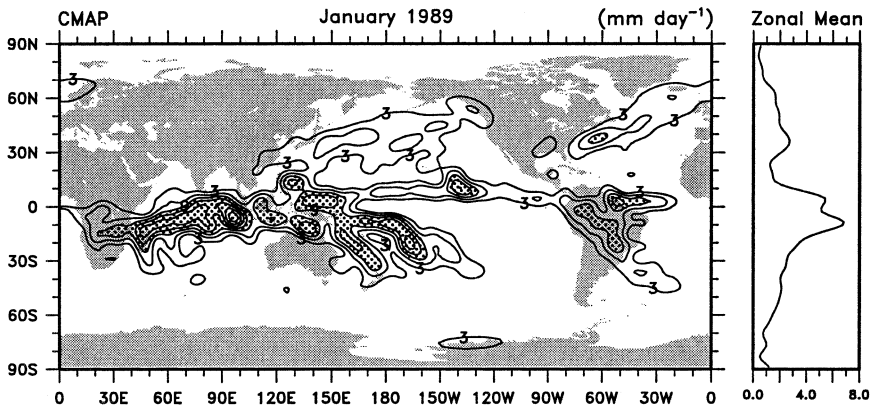

FIG. 5. The precipitation P from Xie–Arkin (1997) in mm day^{-1} at T31 resolution. The contour interval is 3 mm day^{-1}, equivalent to about 87 W m^{-2}, and values greater than 9 mm day^{-1} are stippled. The zonal mean is given at right.

7. There it results in contributions to the energy storage of several tenths of a watt per square meter over high topography (there is no contribution at sea level where $\Phi_s = 0$). Consequently, this term can exceed 1 W m^{-2} over Antarctica, Greenland, and the Himalayas.

The zonal means of the monthly tendency terms in the energy budget (6) as a function of time of year are given in Fig. 9 for the total energy, sensible heat, latent energy, and kinetic energy. The regional maps of the tendency terms for the latent and total energy are given in Figs. 10 and 11. The precipitable water tendency term is typically several tenths of a millimeter per day, which

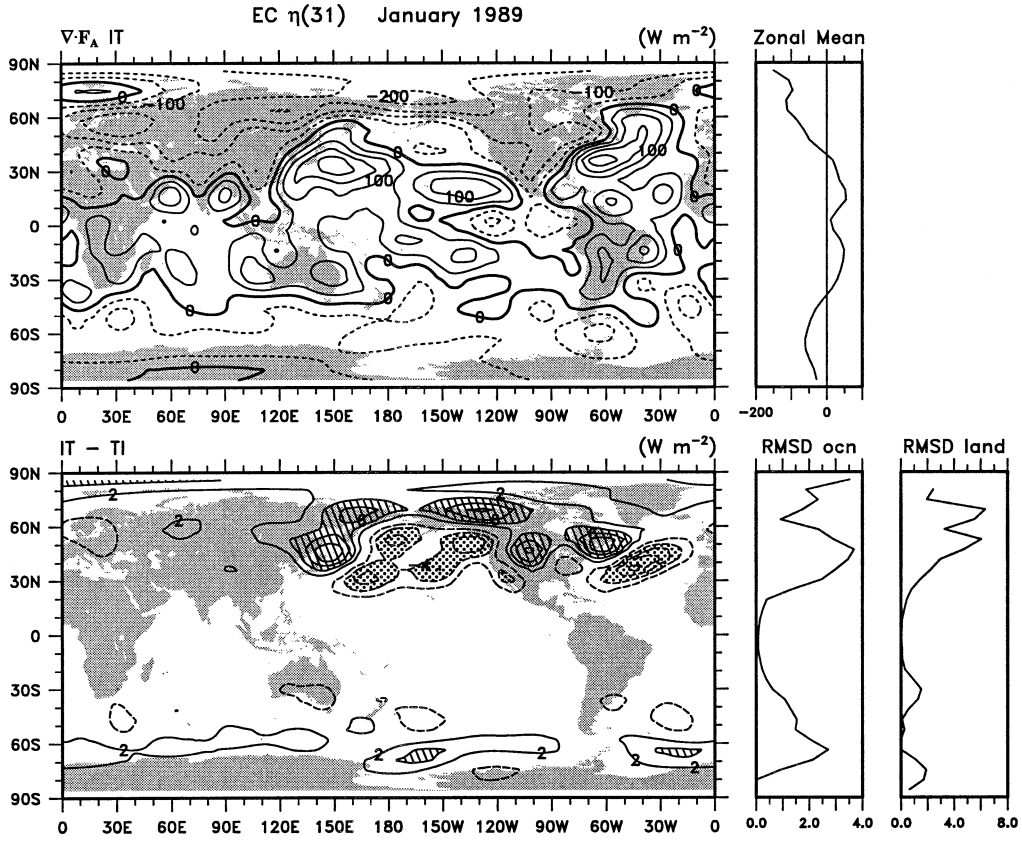

FIG. 6. (top) The $\nabla \cdot \mathbf{F}_A$ from the ECMWF model level archive computed with the vertical integral performed each time before the monthly average is computed (IT), and (bottom) differences from the TI case where the vertical integral is performed after time averaging (Fig. 1b). The contour interval is 50 W m^{-2} in the (top), and 2 W m^{-2} with the zero contour omitted in the (bottom).

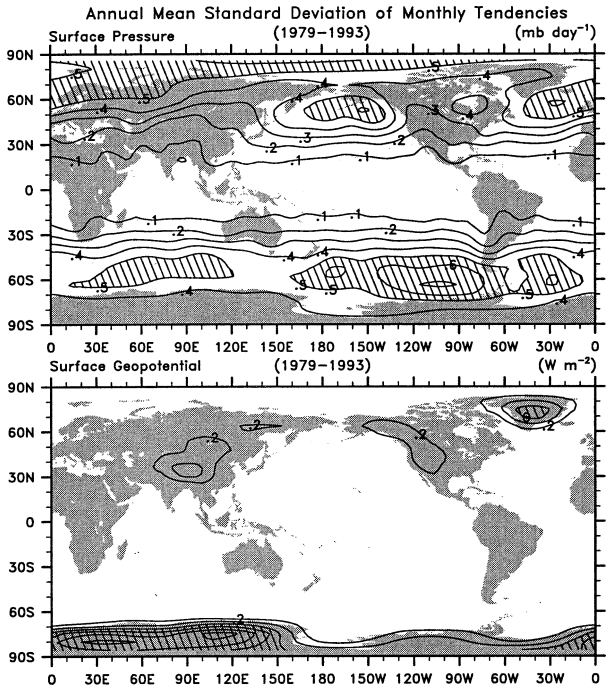

FIG. 7. Annual mean of the std dev of monthly tendency terms for (top) surface pressure, expressed as mb day^{-1} from ERA-15 for 1979–93, values exceeding 0.5 mb day^{-1} are hatched; and (bottom) surface geopotential energy in W m^{-2}, values exceeding 0.6 W m^{-2} are hatched.

is not negligible in the context of the mean values of about 3 mm day^{-1}. It is directly related to the contribution of the latent energy tendency to the energy budget, as 1 mm day^{-1} is approximately 29 W m^{-2}. Naturally, the importance of this term is greatest in the Tropics and subtropics, where Fig. 10 shows that it amounts on average to over 10 W m^{-2} and it exceeds 20 W m^{-2} in the oceanic subtropical regions, such as the SPCZ in summer.

The dominant contribution to the total energy ten-

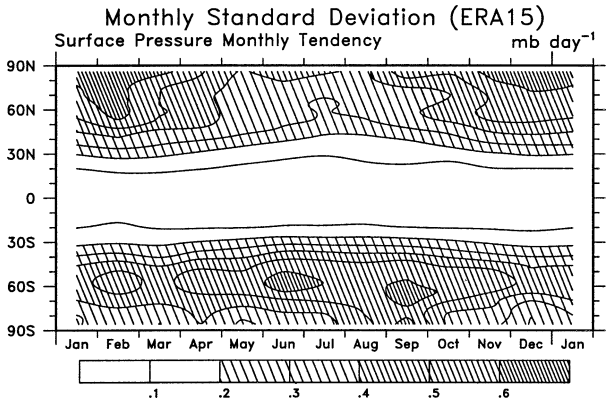

FIG. 8. Annual cycle of the zonal mean of the std dev of monthly surface pressure tendency expressed as mb day^{-1} from ERA-15 for 1979–93.

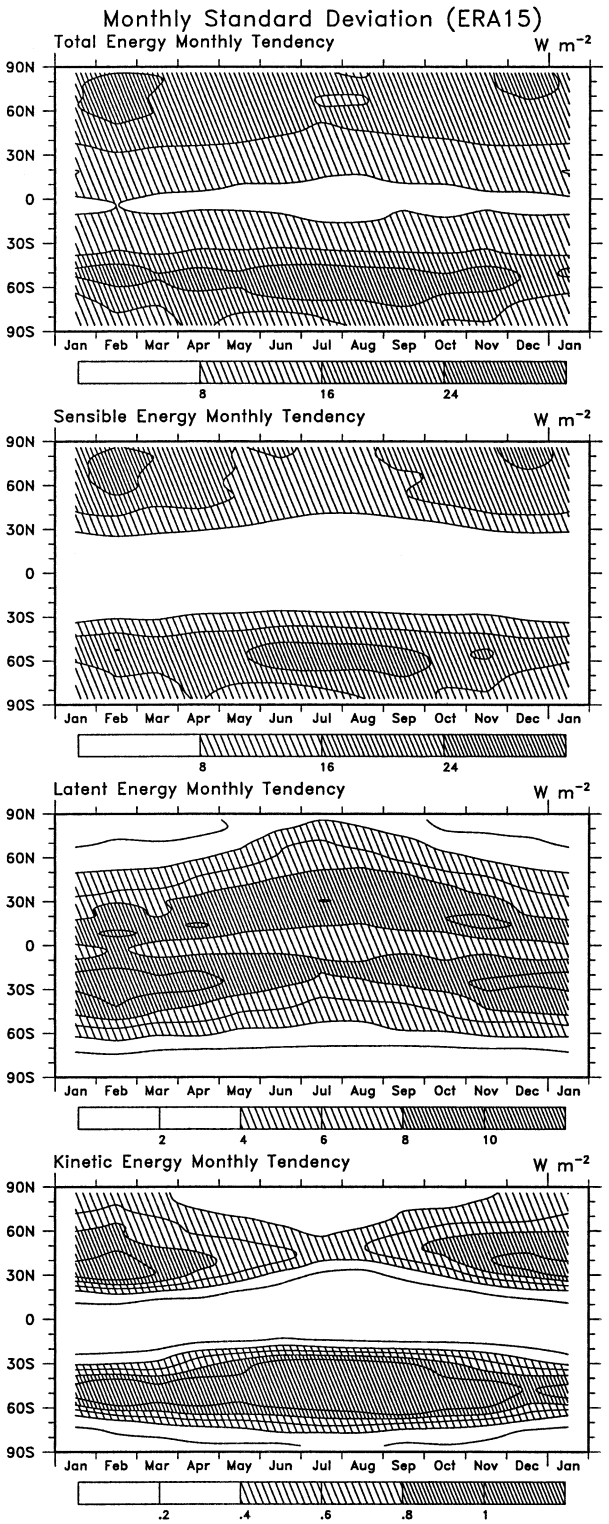

FIG. 9. Annual cycle of the zonal means of std dev of the average monthly tendency terms in the energy budget for the total energy, sensible heat, latent energy, and kinetic energy for 1979–93 (top to bottom, respectively). The units are W m^{-2}.

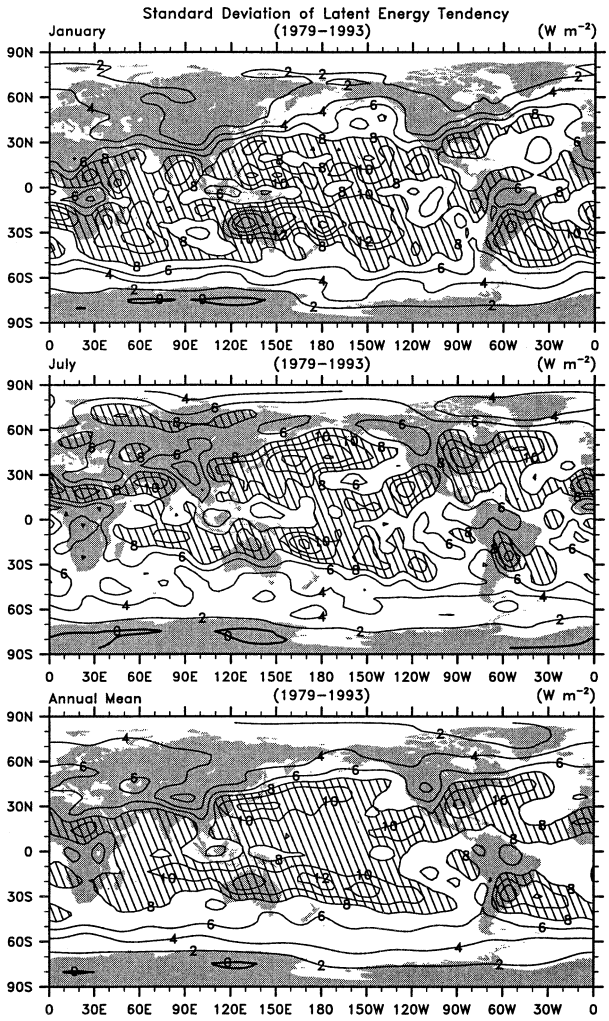

FIG. 10. Std dev of monthly tendencies in latent energy in W m^{-2} for (top) Jan, (middle) Jul, and (bottom) the annual mean for all months. Values exceeding 8 W m^{-2} are hatched.

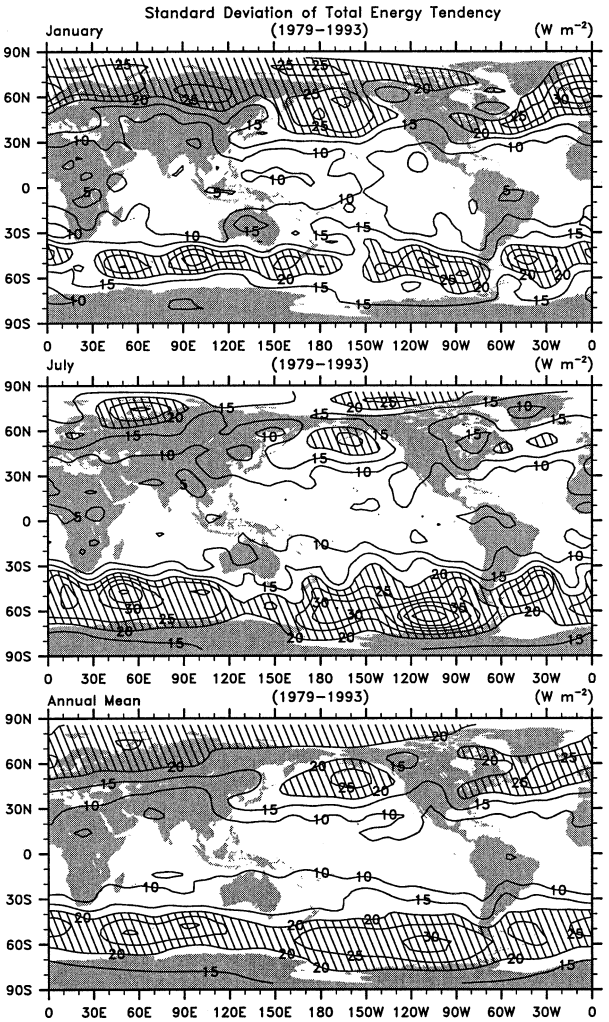

FIG. 11. Std dev of monthly tendencies in total energy in W m^{-2} for (top) Jan, (middle) Jul, and (bottom) the annual mean for all months. Values exceeding 20 W m^{-2} are hatched.

dency, however, comes from the sensible heat (see Fig. 9). Values for both typically exceed 25 W m^{-2} over the oceanic storm track and semipermanent oceanic low pressure regions, such as the circumpolar trough in the Southern Hemisphere and the Icelandic and Aleutian lows in the Northern Hemisphere (Fig. 11). Tendencies in kinetic energy are at least an order of magnitude less (Fig. 9).

6. Pressure coordinates

a. NCEP results

We performed a full set of computations with the NCEP reanalyses in both model and pressure coordinates, with the latter at various resolutions. We had much greater difficulty in replicating the energy budget results with the NCEP pressure archive than from ECMWF, and differences were well in excess of 100 W m^{-2}. Further we traced those differences to the upper layers of the stratosphere and primarily to the term involving the divergence of potential energy, $\nabla \cdot \mathbf{v}\Phi$. While it might be thought that terms in the upper stratosphere would be negligible in an energy budget because the mass weighting is quite small, the geopotential and potential energy become very large, and so this term can be substantial provided that ageostrophic winds are present. The major problems with the NCEP reanalyses in the stratosphere (Trenberth and Stepaniak 2002), are manifested most strongly as a spurious two-delta vertical wave in the divergence of the wind field above steep topography especially where the wind increases with altitude in the stratosphere. The waves are present primarily above 50 mb at the topmost four levels in the NCEP model used for data assimilation and arise from the use of the sigma coordinate system and the upper boundary condition in the assimilating model. Accordingly it is a pathological problem. As it is impossible

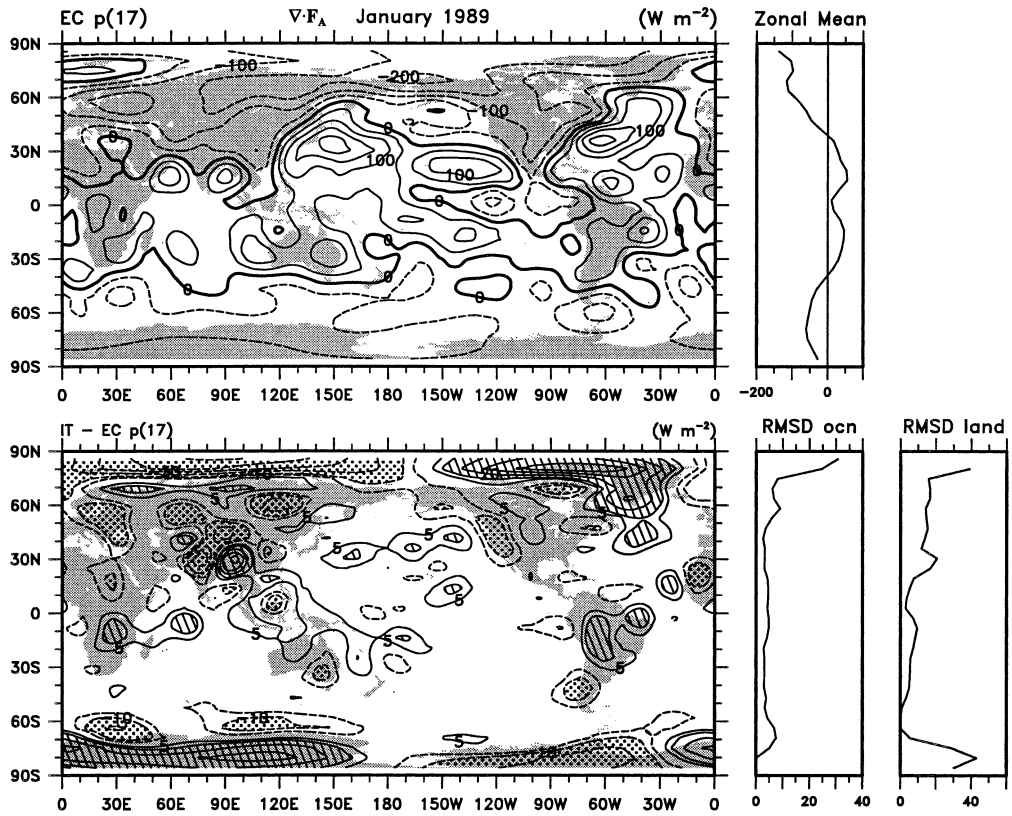

FIG. 12. (top) The $\nabla \cdot \mathbf{F}_A$ from the ECMWF 17-level pressure level archive and (bottom) differences with the IT model level computation in Fig. 6. The contour interval is 50 W m^{-2} in the (top) and contours are ± 5, ± 10, ± 20, . . . , in the (bottom), with values exceeding 10 W m^{-2} hatched and < -10 W m^{-2} stippled. Right panels show the zonal mean (upper) and zonal mean rms differences over the ocean and land (lower).

to address this problem in anything other than the model coordinates, we will not further deal with the NCEP pressure level reanalyses in this paper.

b. ECMWF results

Figure 12 presents the result from the standard ECMWF pressure level archive for $\nabla \cdot \mathbf{F}_A$ and the difference with the model level computation (from Fig. 6). The two fields are quite similar in many respects and differences are relatively modest over most of the oceans. The rms differences along latitude circles (right panels) over the ocean are about 4 versus $\sim$15 W m^{-2} over the northern land areas. Typical differences exceed 10 W m^{-2} in the vicinity of the high-topographic regions of Antarctica, the Tibetan Plateau–Himalayan complex, the Rockies and Greenland, and in the Arctic. Differences are less over South America and Africa.

Examination of the individual terms (not shown) reveals that differences are the order of 5 W m^{-2} in the latent energy over the Tropics and subtropics with zonal mean differences of 2 W m^{-2} at 15°S, and so the main contributor to the differences comes from the dry static energy. Further, both the sensible heat and potential energy terms are large and have strong cancellation between them, but with the error residual coming mostly from the divergence of the transport of the potential energy term in the extratropics.

c. NCAR postprocessor results

Accordingly, we have used our postprocessed pressure level archive to carry out further computations using the ECMWF reanalyses. We first attempted to replicate these results using the NCAR postprocessor at the same vertical resolution, called Np(17), and we are able to replicate the results from the ECMWF pressure level archive quite well (see Fig. 14), with rms differences for $\nabla \cdot \mathbf{F}_A$ less than 5 W m^{-2} over most of the globe. However, there are some important differences at high latitudes, where the Np(17) results appear to be noticeably superior, as discussed further below.

We then added further levels below 700 mb at 725, 750, 800, 825, 875, 900, 950, and 975 mb so that the resolution was 25 mb, and 50 mb elsewhere in the troposphere, giving a 30-level pressure archive, called Np(30). We also tried a similar approach but with 25-mb vertical resolution only below 850 mb with 27 levels and with 25-mb resolution below 600 mb with 32 levels. The results we show are for Np(30). This allows the

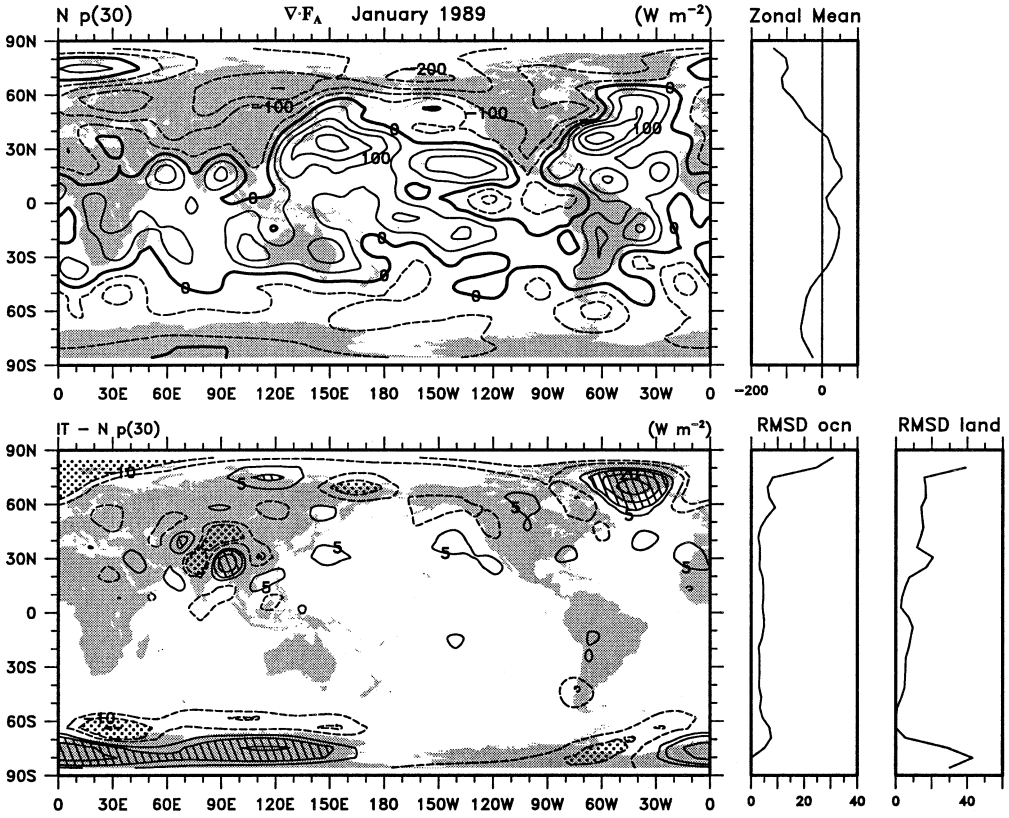

FIG. 13. (top) The $\nabla \cdot \mathbf{F}_A$ from the NCAR postprocessor with 30 pressure levels Np(30) and (bottom) differences with the IT model level computation in Fig. 6. The contour interval is 50 W m^{-2} in the (top) and contours are ± 5, ± 10, ± 20, . . . , in the (bottom), with values exceeding 10 W m^{-2} hatched and less than -10 W m^{-2} stippled. Right panels show the zonal mean (upper), and rms differences over land and ocean (lower).

surface to be mostly defined within a 25-mb layer (except for some parts of Antarctica and the Himalayas) and thereby minimizes contamination from below-ground effects. There was a noticeable improvement in the diagnostics in proceeding from Np(17) to Np(27) in many areas, a modest further improvement in areas of high topography (Antarctica, Himalaya–Tibetan Plateau) for Np(30), but no noticeable change for Np(32) even though surface pressures over parts of Antarctica and in the Himalayas are less than 700 mb. Results from adding extra levels in the mid- and upper troposphere indicated slight improvements in some individual terms, but cancellation of the improvements when summed, and overall errors were much the same.

Figure 13 contrasts results for $\nabla \cdot \mathbf{F}_A$ for the Np(30) archive, which is close to the best achievable with the model-level result. It substantially reduces the discrepancy in the high latitudes (cf. Fig. 12) and the main discrepancies now have a distinct pattern whereby they are associated with high topography. For Np(30), errors in the latent energy term were reduced relative to Np(17) by a factor of 2 or more, indicating the importance of resolving the moisture transports at low levels. Improvements were noted for the two components of the dry static energy, but they largely cancelled in the total. Improvements were most noticeable in areas of significant topography, highlighting the need to resolve where the surface is located. The residual errors that remain in Fig. 13 seem to arise from the divergence of potential energy transports.

Figure 14 summarizes results of comparisons among some of the different options. It shows that most of the differences between the ECp(17) and Np(30) also exist with Np(17), and so stem from the use of a different postprocessor. The NCAR postprocessor is better able to replicate the full model results with 17 levels, and there are some further advantages obtained when the 30-level archive is used. The biggest improvement in going from 17 to 30 levels is near Antarctica where the zonal mean rms differences drop from 20 to 12 W m^{-2}, but differences are mostly less than 4 W m^{-2} elsewhere. The higher vertical resolution gives zonal mean rms differences with the model results of $\sim$5 W m^{-2}, but agreement is excellent over the ocean (mostly less than 3 W m^{-2}) and most of the differences $>$5 W m^{-2} are over or near high topography (Fig. 13). Comparing the ECMWF and NCAR 17-level postprocessing results indicates that the main differences are north of 75°N.

In exploring these discrepancies, we have found prob-

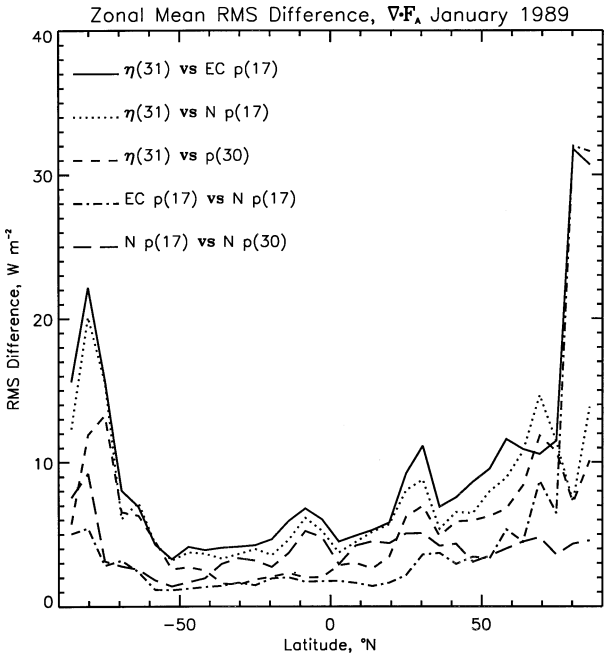

FIG. 14. Rms differences in W m^{-2} taken around each lat circle for $\nabla \cdot \mathbf{F}_A$, comparing results from the IT 31-level model coordinate [η(31) from Fig. 6], ECMWF pressure archive at 17 levels ECp(17), and pressure level archives using the NCAR postprocessor at 17 levels Np(17) and at 30 levels Np(30).

lems with the ECMWF postprocessing.[1] The NCAR postprocessing vertical interpolation is modeled after an earlier version of the ECMWF vertical processing and is quite similar. However, to place values onto a 2.5° grid, the full T106 fields must first be truncated to a compatible resolution to avoid aliasing (Trenberth and Solomon 1993). For the ERA-15 fields, this truncation was performed at T47 and for ERA-40 it will be done at T63. However, we are unable to reproduce the ECMWF results, apparently because of how vector fields were truncated. At NCAR the truncation is performed correctly as a vector pair (Swarztrauber 1993), and results are put out on the 2.5° grid using values computed at each location from the truncated spherical harmonic expansion. At ECMWF, the vectors were truncated as two scalars (actually as a scalar multiplied by $\cos\phi$), and then the latitude–longitude grid values were interpolated from those on the Gaussian grid using bilinear interpolation. A vector field requires an extra mode at each zonal wavenumber compared with a scalar field to properly depict it in spherical harmonics (Trenberth and Solomon 1993). Hence the truncation of a vector as two scalars causes problems at high latitudes (because of the $\cos\phi$ factor), often in wave 1 (see Trenberth and Solomon 1993), and the spatial interpolation causes slight loss of accuracy and loss of invertibility. The effects on the energy budget computation at T42 resolution are the order of 25 W m^{-2}.

d. Sources of errors

The remaining errors seem to partly arise from large discrepancies between the sum of c_pT and gz transports below ground, and relate to the ways that temperature, geopotential, and wind are extrapolated below ground. In pressure coordinates, it is inevitable that some contamination from this enters the diagnostic calculations because the surface is not located to better than a 25-mb layer even in our best computation.

At each grid point we make use of the surface pressure. All full layers above there are included in the vertical integral while the ''surface layer'' is weighted by the appropriate amount, and all layers below are omitted. However, this means that the surface layer contains some information from below ground. The worst case for a 25-mb layer is when the surface pressure is halfway in between the levels, so that the mass weighting is for a 12.5-mb layer with half of the information from below ground.

In the Himalayan region in January, the mountains are elevated cold areas relative to the free atmosphere and there is a large diurnal cycle of temperature at the surface and below ground (e.g., about ± 8°C at 850 mb), but with a much smaller diurnal cycle in geopotential height, so that the dry static energy mostly follows the diurnal cycle of temperature. It seems likely that this imbalance contributes to the errors that remain. Changes in the way extrapolation below ground is performed might help (e.g., by horizontal interpolation), but this could also be counterproductive for other uses of the data.

7. Conclusions

We have carefully analyzed the various contributions to the total energy budget and noted the very large cancellation among several terms that require consistent numerical approaches in order to avoid large errors. Within the dry static energy, there is large cancellation between the potential energy and sensible heat terms that arises from the almost isentropic nature of many motions in the absence of precipitation. Additional cancellation arises between the moist (or latent) energy component and the dry static energy, which is similarly related to the relevance of moist adiabatic processes, as discussed in section 3. A substantial mass balance correction is essential to obtain accurate results. Experience shows that ensuring a mass balance also compensates remarkably well for shortcomings in temporal sampling (Trenberth 1997), which in all cases was 4 times daily. Tendencies of the storage of the various energy components are large enough (several tens of watts per square meter) to require careful attention on monthly timescales. We further argue that the key diagnostic we

[1] These have now been confirmed by ECMWF.

have used, namely, $\nabla \cdot \mathbf{F}_A$, is an important one as it relates directly to the diabatic forcings of the atmosphere, and thus can be used to check against model parameterizations.

Many formulations of heat and energy balances in diagnostic computations are not accurate as they do not use the correct equations, especially in some mesoscale studies. Most frequently, the kinetic energy equation is ignored and an equation for the dry or moist static energy is included but no such expression exists without approximations (e.g., Tian et al. 2001). In addition, it is very misleading to focus on only one of the components when they are dynamically linked. Another common error is to interpret a flux of energy as a transport without ensuring a closed mass circulation. Thus, examining only the upper branch of the Hadley circulation and the implied energy transports without also considering the return flow branch at lower levels and typically different energy (as in Tian et al. 2001) is also wrong. Only integration over a closed mass circulation makes physical sense for energy and heat transports, as otherwise there is a missing component, required by mass continuity, that is not taken into account.

In the course of this diagnostic investigation, we uncovered major problems in the NCEP reanalyses in the stratosphere that are inherent in the model formulation (Trenberth and Stepaniak 2002). This made them unsuitable for quantitative use in anything other than model coordinates. In addition, we have revealed small flaws in the postprocessing procedures by ECMWF in producing their pressure level archive. These stem from the way the vector fields are truncated, which is a necessary step to avoid aliasing before putting the values out on a 2.5° grid. Moreover, it is highly desirable to compute the gridpoint values exactly rather than interpolating them from the Gaussian grid as currently done by ECMWF. NCEP postprocessing may also have problems, and our computations raise questions about vertical interpolation procedures and the manner in which the layers are defined (see Table 1). For NCEP reanalyses on a 2.5° grid, no horizontal truncation is necessary as the model reanalyses are at T62.

Trenberth and Caron (2001) found larger northward energy transports in the atmosphere from NCEP compared with ECMWF and these were superior in terms of the overall energy budget when compared with estimates of the ocean heat transports. Here we find for January 1989 that a substantial part of these differences stems from the latent energy transport, which has a greater southerly component as the greater evaporation in the subtropics of the Northern Hemisphere results in moisture being transported southward into the intertropical convergence zone, and especially into the SPCZ and Southern Hemisphere monsoons (Fig. 4). Hence, it is related to the too vigorous hydrological cycle in the ERA-15 (Stendel and Arpe 1997).

The diagnostic results shown here and computed with our own postprocessor have resulted in a pressure level archive created with 30 levels that can replicate the full model level results to within about 2 W m^{-2} over the ocean for $\nabla \cdot \mathbf{F}_A$, and with errors exceeding 10 W m^{-2} in small spots over Greenland, Antarctica, and the Himalayan–Tibetan Plateau complex. The latter are regions where the terrain-following coordinate is compressed above high topography thereby providing much higher model resolution than possible in a pressure level archive. But they are also regions where model numerics run into trouble through truncation and other errors (see Trenberth and Stepaniak 2002).

There is clear evidence that the standard pressure level archive is far too coarse in terms of vertical resolution to resolve the surface and boundary layer adequately. On the other hand, for many purposes, the model coordinate is not suitable because it varies in time with surface pressure, and the number of levels is many more than required for diagnostic purposes. To partition quantities in the vertical it is much more desirable to use pressure coordinates than a time-varying coordinate. Also a common coordinate is essential if models are to be compared with one another and with observations, and again the best choice is pressure. We suggest that a future pressure archive more suitable for quantitative diagnostics should contain the following 30 levels in addition to any enhanced resolution in the stratosphere: p = 1000, 975, 950, 925, 900, 875, 850, 825, 800, 775, 750, 725, 700, 650, 600, 550, 500, 450, 400, 350, 300, 250, 200, 150, 100, 70, 50, 30, 20, and 10 mb. This increases the resolution to 25 mb below 700 mb, 50 mb through the main troposphere, and includes the 20-mb level in the stratosphere. Consideration should also be given to including a 1025-mb level. We also call for much improved documentation of postprocessing procedures by the operational centers, simply in order to be able to determine what has been done.

Acknowledgments. This research was sponsored by grants from NOAA Office of Global Programs and jointly by NOAA–NASA under NOAA Grant NA17GP1376. We thank Per Kållberg and Adrian Simmons for help with the ECMWF reanalyses.

REFERENCES

CLIVAR, 1998: The CLIVAR initial implementation plan. WMO/TD 869, WCRP 103, ICPO 14, 356 pp.

Emanuel, K. A., 1995: On thermally direct circulations in moist atmospheres. *J. Atmos. Sci.,* **52,** 1529–1534.

Gibson, J. K., P. Kållberg, S. Uppala, A. Hernandez, A. Nomura, and E. Serrano, 1997: ERA description. ECMWF Reanalysis Project Rep. 1, 72 pp.

Johnson, R. H., and P. E. Ciesielski, 2000: Rainfall and radiative heating rates from TOGA COARE atmospheric budgets. *J. Atmos. Sci.,* **57,** 1497–1514.

Kalnay, E., and Coauthors, 1996: The NCEP/NCAR 40-Year Reanalysis Project. *Bull. Amer. Meteor. Soc.,* **77,** 437–471.

Oort, A. H., 1978: Adequacy of rawinsonde network for global circulation studies tested through numerical model output. *Mon. Wea. Rev.,* **106,** 174–195.

——, and J. P. Peixoto, 1983: Global angular momentum and energy

balance requirements from observations. *Advances in Geophysics,* Vol. 25, Academic Press, 355–490.
Stendel, M., and K. Arpe, 1997: Evaluation of the hydrological cycle in reanalyses and observations. Max-Planck-Institut für Meteorologie Rep. 228, 52 pp.
——, J. R. Christy, and L. Bengtsson, 2000: Assessing levels of uncertainty in recent temperature time series. *Climate Dyn.,* **16,** 587–601.
Swarztrauber, P. N., 1993: The vector harmonic transform method for solving partial differential equations in spherical geometry. *Mon. Wea. Rev.,* **121,** 3415–3437.
Tian, B., G. J. Zhang, and V. Ramanathan, 2001: Heat balance in the Pacific warm pool atmosphere during TOGA COARE and CEPEX. *J. Climate,* **14,** 1881–1893.
Trenberth, K. E., 1991: Climate diagnostics from global analyses: Conservation of mass in ECMWF analyses. *J. Climate,* **4,** 707–722.
——, 1995: Truncation and use of model-coordinate data. *Tellus,* **47A,** 287–303.
——, 1997: Using atmospheric budgets as a constraint on surface fluxes. *J. Climate,* **10,** 2796–2809.
——, and A. Solomon, 1993: Implications of global atmospheric spatial spectra for processing and displaying data. *J. Climate,* **6,** 531–545.
——, and C. J. Guillemot, 1998: Evaluation of the atmospheric moisture and hydrological cycle in the NCEP/NCAR reanalyses. *Climate Dyn.,* **14,** 213–231.
——, and J. M. Caron, 2001: Estimates of meridional atmosphere and ocean heat transports. *J. Climate,* **14,** 3433–3443.
——, and D. P. Stepaniak, 2002: A pathological problem with NCEP reanalyses in the stratosphere. *J. Climate,* **15,** 690–695.
——, ——, and J. M. Caron, 2000: The global monsoon as seen through the divergent atmospheric circulation. *J. Climate,* **13,** 3969–3993.
——, J. M. Caron, and D. P. Stepaniak, 2001a: The atmospheric energy budget and implications for surface fluxes and ocean heat transports. *Climate Dyn.,* **17,** 259–276.
——, D. P. Stepaniak, J. W. Hurrell, and M. Fiorino, 2001b: Quality of reanalyses in the Tropics. *J. Climate,* **14,** 1499–1510.
Xie, P., and P. A. Arkin, 1996: Analyses of global monthly precipitation using gauge observations, satellite estimates, and numerical model predictions. *J. Climate,* **9,** 840–858.
——, and ——, 1997: Global precipitation: A 17-year monthly analysis based on gauge observations, satellite estimates, and numerical model outputs. *Bull. Amer. Meteor. Soc.,* **78,** 2539–2558.
Yanai, M., and T. Tomita, 1998: Seasonal and interannual variability of atmospheric heat sources and moisture sinks as determined from NCEP–NCAR reanalyses. *J. Climate,* **11,** 463–482.
——, S. Esbensen, and J.-H. Chu, 1973: Determination of bulk properties of tropical cloud clusters from large-scale heat and moisture budgets. *J. Atmos. Sci.,* **30,** 611–627.
——, J.-H. Chu, T. E. Stark, and T. Nitta, 1976: Response of deep and shallow tropical maritime cumuli to large-scale processes. *J. Atmos. Sci.,* **33,** 976–991.
Yu, R., M. Zhang, and R. D. Cess, 1999: Analysis of the atmospheric energy budget: A consistency study of available data sets. *J. Geophys. Res.,* **104,** 9655–9661.